# Fluorescence measurement by a streak camera in a single-photon-counting mode

**ARTICLE** *in* PHOTOSYNTHESIS RESEARCH · AUGUST 2009

Impact Factor: 3.5 · DOI: 10.1007/s11120-009-9463-x · Source: PubMed

Photosynth Res (2009) 101:119–133
DOI 10.1007/s11120-009-9463-x

REVIEW

# Fluorescence measurement by a streak camera in a single-photon-counting mode

**Masayuki Komura · Shigeru Itoh**

Received: 17 February 2009 / Accepted: 15 June 2009 / Published online: 1 July 2009


**Abstract** We describe here a recently developed fluorescence measurement system that uses a streak camera to detect fluorescence decay in a single photon-counting mode. This system allows for easy measurements of various samples and provides 2D images of fluorescence in the wavelength and time domains. The great advantage of the system is that the data can be handled with ease; furthermore, the data are amenable to detailed analysis. We describe the picosecond kinetics of fluorescence in spinach Photosystem (PS) II particles at 4–77 K as a typical experimental example. Through the global analysis of the data, we have identified a new fluorescence band (F689) in addition to the already established F680, F685, and F695 emission bands. The blue shift of the steady-state fluorescence spectrum upon cooling below 77 K can be interpreted as an increase of the shorter-wavelength fluorescence, especially F689, due to the slowdown of the excitation energy transfer process. The F685 and F695 bands seem to be thermally equilibrated at 77 K but not at 4 K. The simple and efficient photon accumulation feature of the system allows us to measure fluorescence from leaves, solutions, single colonies, and even single cells. The 2D fluorescence images obtained by this system are presented for isolated spinach PS II particles, intact leaves of *Arabidopsis thaliana*, the PS I super-complex of a marine centric diatom, *Chaetoceros gracilis*, isolated membranes of a purple photosynthetic bacterium, *Acidiphilium rubrum*, which contains Zn-BChl *a*, and a coral that contains a green fluorescent protein and an algal endosymbiont, *Zooxanthella.*

M. Komura · S. Itoh (✉)
Division of Material Science (Physics), Graduate School of Science, Nagoya University, Furocho, Chikusa, Nagoya 464-8602, Japan
e-mail: itoh@bio.phys.nagoya-u.ac.jp

**Keywords** Streak camera · Photosystem II · Excitation energy transfer · Time-resolved fluorescence spectroscopy · Chlorophyll fluorescence · Global analysis · Temperature dependency

**Abbreviations**

| | |
|---|---|
| CCD | Charge coupled device |
| DAS | Decay-associated spectrum |
| EET | Excitation energy transfer |
| F685, F695 and F735 | Fluorescence bands peaking at 685, 695, and 735 nm respectively |
| LHC | Light-harvesting chlorophyll *a*/*b* binding complex |
| MCP | Multichannel plate |
| P680 | Primary electron donor in PS II |
| PS | Photosystem |
| RC | Reaction center |

## Introduction

Fluorescence lifetimes have been measured by the direct detection of the decay kinetics, phase fluorimetry, the time correlated photon-counting method, or an up-conversion method. These measurements have been widely used and are highly developed by the use of ultra-rapid laser excitation light sources. We describe here a recently developed measurement system using a streak camera in a single-photon-counting mode together with the analysis that is common for other systems. For a background on the Chlorophyll (Chl) fluorescence and the lifetime of the Chl fluorescence, see books edited by Govindjee et al. (1986) and Papageorgiou and Govindjee (2004). For the fluorescence measurement by

a streak camera single-photon-counting method, see reviews by Itoh and Sugiura (2004) and Gilmore (2004).

A streak camera is a vacuum tube designed to convert fast time intervals to differences in the geometry by flowing photo-induced electrons under a rapid-scanning electric field (Fleming et al. 1977; see the homepage of Hamamatsu Photonics, http://learn.hamamatsu.com/tutorials/streakcamera/). Such a tube had been used to detect fast photoevents by recording real-time images of the output with a video camera. At that stage, the streak camera was specifically used for very rapid processes that had a sufficient amount of photons to be measured directly, such as in ultra-fast absorption changes (Ito et al. 1991). The streak camera has an advantage over the photomultiplier tube, since it has a faster response time (up to 0.1 ps) and 2D-conversion capability. However, it was not very popular for the measurement of fluorescence lifetimes due to its analog nature compared to the digital time correlated photon-counting method, which had been widely used and developed together with the fast response photomultiplier or multichannel plate. The development of the photon-counting mode in the streak camera system renders it a highly convenient modern detection system with high sensitivity and a fast time response. This was enabled by the use of a charge coupled device (CCD) camera as the final-recording system, fast image transfer, and fast data processing with computers.

In this review, we describe a convenient streak camera system that is rather expensive (available from starting at US $200,000), but is excellent as a small, nearly all-in-one system when used with a laser diode that gives a 50-ps flash of different colors. The system is more useful when coupled with the use of femtosecond laser sources. It allows direct 2-dimensional (2D) detection of spectrum-time images obtained on the basis of photon-counting principle. The advantages of conducting measurements using this system are: (1) the detection of both wavelength and time from the same shot of a laser pulse. This prevents artifacts due to spectrum/decay changes during long measurements and (2) the efficient capture of almost all photons emitted at different wavelengths and times. The disadvantage might be a rather slow cycling time for scan of an electrical field (about 1 microsecond for a 2 ps streak camera and longer for a streak camera with faster time resolution). The other disadvantage might be that at present there is only one supplier of streak cameras: Hamamatsu Photonics (Hamamatsu, Japan).

X-ray crystallography studies on Photosystem I (PS I), Photosystem II (PS II), and several Chl-binding proteins have been reported in the past decades. The structures of trimeric PS I and dimeric PS II of thermophilic cyanobacteria were resolved at 2.5 and 2.9 Å resolutions, respectively (Jordan et al. 2001; Guskov et al. 2009). One PS I unit binds 96 Chls, 2 phylloquinones, 3 FeS clusters, 22 carotenoids, and several other cofactors. All cofactors including electron transfer components are located in two large core subunits called PsaA and PsaB. On the other hand, 77 cofactors, including 35 Chls, 2 pheophytins, 2 plastquinones, and 11 carotenoids, were resolved in one PS II unit (Loll et al. 2005; Guskov et al. 2009). In higher plants, the PS I complex is monomeric and is surrounded by four peripheral antenna proteins called the light-harvesting chlorophyll *a*/*b* binding protein complex (LHC) I (Amunts et al. 2007); there are 168 Chls in the entire PS I system. The central core of the reaction center (RC) of PS II, which is made of D1 and D2 subunit proteins, is rather small and binds two core antenna proteins called CP43 and CP47. Although the molecular structure of PS II in higher plants has not been resolved, it seems to be surrounded by a number of LHC IIs to form a PS II-LHC II super-complex (Boekema et al. 1999). Each PS II-LHC II super-complex has more than 200 Chls in total. The photon energy absorbed by Chls on the complex is efficiently transferred to the Chls on the RC moiety and used for charge separation.

Picosecond/subpicosecond-time-resolved Chl fluorescence decay kinetics has been extensively studied to understand the mechanism of excitation energy transfer in PS I and II (Dekker and van Grondelle 2001; Gobets and Van Grondelle 2001; Melkozernov 2001). At room temperature, excitation energy transfer (EET) occurs within 10 ps from bulk Chls emitting at 680–690 nm to the so-called red Chls, which emit fluorescence beyond 700 nm in PS I. The excitation-trapping process has been suggested to occur in a few to tens of picoseconds on P700 (Gobets et al. 2001; Ihalainen et al. 2005; Slavov et al. 2008). In contrast, PS II exhibits a single fluorescence peak at around 685 nm (Dekker et al. 1995; Andrizhiyevskaya et al. 2005). This makes it difficult to resolve EET processes in PS II at room temperature. The details of the EET process from the outer antenna Chls to the Chls in the central moiety are, therefore, still being debated (Andrizhiyevskaya et al. 2004; Broess et al. 2006; Miloslavina et al. 2006).

On cooling the samples, the 685-nm fluorescence peak shifts to the red and then turns into two distinct peaks at 685 and 695 nm below 100 K, named F685 and F695, respectively (Brody and Brody 1963; Cho et al. 1966; Krey and Govindjee 1964; Govindjee and Yang 1966; Murata et al. 1966). Rapid EET between these two bands are assumed even at 77 K (Gasanov et al. 1979; Mimuro et al. 1987). The F695 seems to be emitted from Chl *a* in CP47 (Dorssen et al. 1987a, b; Dekker et al. 1995; De Weerd et al. 2002a), and F685, from Chl *a* in CP43 (Dorssen et al. 1987a). The excitation energy seems to be transferred to the RC moiety by a slightly uphill process (De Weerd et al. 2002b). Below 77 K, the fluorescence intensity increases together with the blue shift of the spectrum (Cho and

Govindjee 1970a, b, Masters et al. 2001; Krausz et al. 2005). The isolated PS II RC complex gives a single fluorescence peak at 684 nm at 4 K (Groot et al. 1994). The isolated CP43 and CP47 show single peaks at 683 and 691 nm, respectively, at 4 K (Dekker et al. 1995; Groot et al. 1995, 1999). Therefore, the blue shift that is opposite to the red shift detected on cooling to 77 K is rather difficult to be interpreted as thermal re-distribution of the excitation energy among the different energy levels of Chl bands, as seen in the case of PS I fluorescence (Croce et al. 2000).

As a typical experimental example, we describe here the picosecond kinetics of fluorescence in spinach PS II particles at 4–77 K measured by a streak camera system using a liquid-helium cryostat unit. We first calculated the decay associated spectrum (DAS) which indicates the rise and decay of fluorescence at different wavelengths. We then performed a global multi-Gaussian fitting analysis of time-resolved fluorescence spectra calculated from the same data set to determine the precise peak positions and the decay profiles of component bands. This method provided clear information on the temperature dependencies of the rise and decay of each component band and identified a new fluorescence emission band, F689, which becomes prominent only below 77 K (Komura et al. 2006). The temperature dependency of the EET dynamics in intact PS II is discussed here on the basis of the new results. These results shed light on the uphill EET process at 4 K that had been interpreted, earlier, by the models with only F685 and F695 bands (Andrizhiyevskaya et al. 2005; Krausz et al. 2005).

The 2D fluorescence images obtained by this system are also presented later in this review for various photosynthetic systems, i.e., an intact leaf of *Arabidopsis thaliana*, a PS I super-complex isolated from a marine centric diatom, *Chaetoceros gracilis*, membranes from a purple photosynthetic bacterium, *Acidiphilium rubrum*, which contains Zn-BChl *a*, and an intact coral that contains a green fluorescent protein and an algal endosymbiont, *Zooxanthella.*

## A streak camera system for the measurement of fluorescence decay and spectrum

Figure 1 shows a schematic presentation of the streak camera system currently used (available from Hamamatsu Photonics). The system consists of a streak camera, laser sources, and a sample compartment.

The use of a laser diode allows us to excite at 405, 630, 645, or 820 nm. Although the wavelength range of laser

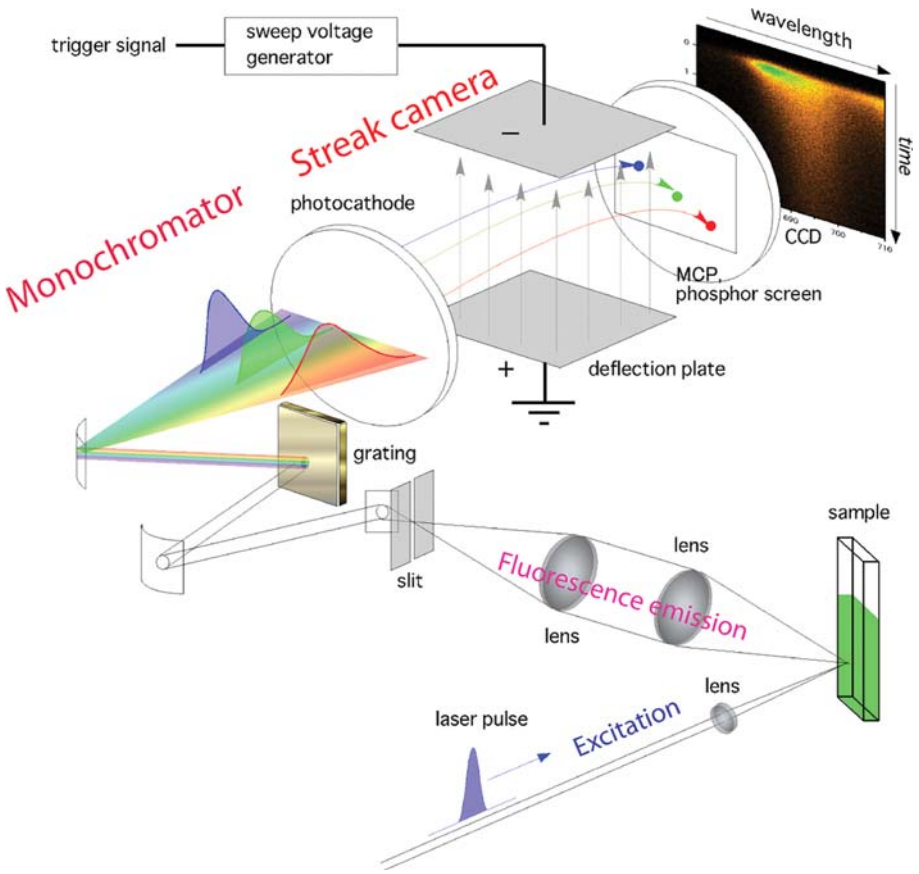


**Fig. 1** Schematic presentation of the streak camera fluorescence measurement system. See text for the details

diodes is currently increasing, the 50–60 ps duration of a diode laser pulse still limits the time resolution of the whole system. Use of the 150 fs laser pulse from a Ti:Sapphire laser greatly increased the time resolution of the system and limited it only by the response of the steak camera itself.

The wavelength–time 2D images obtained by the system give information for the time domain in addition to the spectral domain. Even when we do not need specific decay time constants, we can easily detect the different lifetimes, such as in the spectra, directly from the images. This instant and easy feature allowed us to measure the effects of mutations or sample conditions. The system allows the easy measurement of the fluorescence spectra as well as its time dependence. The simple setup and efficient photon accumulation features of the system make it possible to measure fluorescence from leaves, suspensions of cells and chloroplasts, pigment-proteins, and single colonies. The fluorescence decay from a single cell was measured when the system was combined with a confocal microscope.

## Overview of the system

As mentioned above, Fig. 1 shows a schematic presentation of a streak camera system (Hamamatsu 4334; Hamamatsu Photonics, Inc., Hamamatsu, Japan) that consists of a pulse laser, a sample compartment, a monochromator, and a streak camera system. The sample can also be set in a liquid nitrogen or liquid-helium cryostat to measure low-temperature fluorescence. The whole system with a laser diode is rather compact (0.6 m $\times$ 1.2 m).

## Excitation laser

The excitation flashlight was provided by a laser diode emitting at 405 nm (with a 50-ps pulse width and operated at 1 MHz, Hamamatsu Photonics, Inc., Hamamatsu, Japan) that passed through a 405-nm interference filter. The excitation source can be replaced with diode lasers at other wavelengths, such as 630, 645, or 820 nm, if required. The shorter pulse light from femtosecond lasers, such as the 355–460 nm second harmonic of the Ti:Sapphire laser (in our case Mai Tai, Spectra Physics) gave better resolution of time, as expected. The stray light or scattering of a laser pulse is eliminated by the use of appropriate optical filters. Attention should be paid to prevent the disturbance due to the fluorescence from these filters.

## Monochromator

The laser excitation beam was focused on the sample surface to give a spot as small as possible with a diameter of less than 1 mm. Fluorescence emitted from the spot was carefully focused onto the entrance slit of a monochromator (50 cm Chromex 2501-S; Hamamatsu Photonics, Hamamatsu, Japan) with a slit width of less than 40 μm through an appropriate cutoff filter that eliminates the laser scattering light. Proper focusing is carefully achieved in three dimensions by the use of reference materials because it is important to obtain high spectral and time resolution. For instance, we observe four spots of the laser scattering from the two surfaces of the outer and inner glass plates of the sample cuvette as well as the sample fluorescence. On the other hand, if we put a leaf section without a cover glass plate, we can observe a single spot of laser scattering overlapping with sample fluorescence. We chose one of the three gratings that are built in the monochromator. In a typical case for the PS II measurement, we use a grating with 100 grooves $mm^{-1}$ blazed at 780 nm to give a center wavelength of 700 nm with a 150 nm wavelength range and a spectral resolution of 3.3 nm.

## Streak camera

The light from the exit slit of the monochromator is guided to the photocathode at the entrance of the streak camera to give a horizontal linear spectral image. The photoelectrons produced are further accelerated by the electrical field and biased to the vertical direction under a variable electrical field. The later the arrival time, the higher the electrical field to give a larger vertical displacement. The field scan and the laser flashing are controlled by a common timing generator. The photoelectrons hit the multichannel plate (MCP) inside the streak camera and produce multiple electrons that give a single spot on the target phosphor screen. Then the spot is recorded by CCD (Charge Coupled Device). The CCD image that accumulated these spots is then transferred to a computer every 33 ms.

## Charge coupled device (CCD) coupling

The CCD image with a 640 horizontal $\times$ 480 vertical pixels records the 2D (wavelength and arrival time) position of each photon emitted from the sample. Although the apparent shortest time resolution along the vertical axis can be 1 ns/480 = 2.1 ps for the fastest scan range of 1 ns in our case, it is actually around 5 ps or even longer due to the cross talks between pixels. The trace of the multiple photoelectrons induced by a single-photon is also much larger than one pixel. The size and intensity of each spot actually fluctuates due to the fluctuations of the production and amplification of photoelectrons. The spot intensities are, however, stronger than the thermally activated noise levels. Therefore, the adaptation of the photon-counting principle for the CCD

image significantly increases the signal/noise ratio, as in the case of traditional single-photon-counting technique. We first measure the level of thermal noise and determine a certain threshold level. We then count the location of the spot that gives the intensity beyond the threshold level. As for the location of the photon, we either use the highest peak position or the center of gravity calculated by a computer. Care is also taken to attenuate the fluorescence intensity to suffice the single-counting principle for each image taken every 33 ms. Attention is paid to avoid double-photon events on one spot on the image, as in the case of all photon-counting techniques. The amount of photons into the streak camera must be controlled by the attenuation of either the laser power or the fluorescence intensity.

2-dimensional imaging

We counted locations of photons in the single-photon-counting mode and accumulated them on the wavelength/time 2D space as shown in Fig. 2. This allowed us to acquire a 2D fluorescence image typically in a 150-nm wavelength range in the horizontal axis and a 1–1,000 ns vertical time axis in a 640 × 480 point image. The 2D images presented in this article were obtained after 0.5–2 h accumulations. The fluorescence bands of Chl give wide horizontal bands that last for some time (Fig. 2b, c), while the scattering of excitation laser gives a small spot (Fig. 2a), showing its narrow bandwidth and short duration. Fluctuations in the scanning and laser firing timings, the focusing extent, or stray light can be easily checked in a real-time mode, which does not accumulate locations, or in a focusing mode, which stops the time scanning of the streak camera.

## Experimental conditions

The conventional high-efficiency single-photon-counting method with the streak camera allows us to use a relatively low intensity laser for the excitation. The diode lasers, thus, are suited because of their low intensity, controllable repetition rate, and high cost performance. They give another benefit of avoiding photo-damage to the biological samples. With diode laser excitation at room temperature, severe damage to samples is generally avoided. Thus, we could use a single leaf or even a single colony for a one-hour measurement without significant damage and with good reproducibility.

The measurement with the streak camera gives 2D images obtained directly by single-photon counting. The data are used to form a 2D histogram and provide reliable profiles for wavelength and lifetime. This situation is advantageous to the other types of traditional fluorimetry that are first used to obtain a time profile of fluorescence at each wavelength and then to scan the wavelength and collect data for a long time. The result obtained with the streak camera can be almost free from the drift of irradiation laser intensity and from the dynamic range of the streak camera and CCD themselves because of the photon-counting principle. Data could also be saved several times after short exposure times, and time-dependent changes of spectra and decay time courses due to the time-dependent variation of sample conditions could be recorded.

Different sensitivity/photon energy at different emission wavelengths does not significantly affect the spectrum calculated on the basis of the single-photon-counting principle if the threshold value for the photon-counting is properly chosen. Calibration of the spectral sensitivity was done by measuring the emission from the standard tungsten

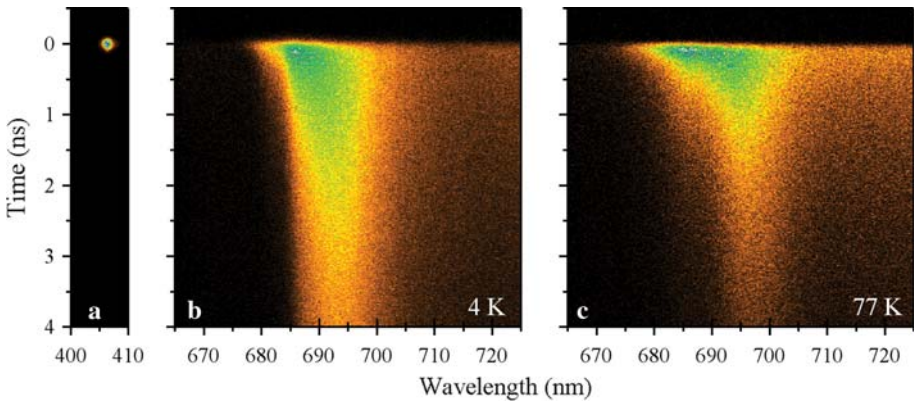


**Fig. 2** Typical wavelength–time 2D fluorescence decay images obtained from spinach PS II particles. **a** Scattering of the laser diode excitation flash at 405 nm (with a 50-ps pulse width). **b** and **c** Fluorescence from PS II particles at 4 K (**b**) and 77 K (**c**). Measurements were done in the 5 ns window time. The vertical axis represents the time with respect to the excitation flash. The horizontal axis represents the fluorescence emission wavelength. The excitation source was a 405-nm laser diode operated at 1 MHz as seen from (**a**). See text for details

lamp in the photon-counting mode, as is widely used for the calibration of the fluorescence spectrum in ordinary fluorimetry.

### Materials

Solution (or suspensions) of the isolated RCs or antenna proteins, suspensions of cell or membranes, intact leaves, colonies of cells on agar plates, and even living corals can be used as samples as long as they can be placed before the lens in front of the monochromator entrance, as used in an ordinary fluoroscope. We can collect fluorescence from a small spot on the sample surface efficiently. If the monochromator entrance is coupled to fiber and the laser output is also coupled to the fiber, then the excitation and collection of fluorescence can be performed only with the fibers. However, in this case, we must pay attention to the difference in the speed of light at different wavelengths inside the long fibers. The redder the emission, the slower the arrival time.

The PS II particles (Berthold Babcock Yocum (BBY) - type) used in this study were prepared from spinach, as reported (Berthold et al. 1981), with some modifications (Ono and Inoue 1986; Mino and Itoh 2005). These PS II particles were suspended in a medium containing 0.4 M sucrose, a 20-mM MES buffer (pH 6.5), and 20 mM NaCl and used for spectroscopy. Glycerol was added to give a final concentration of 60% for measurements at low temperature. The dark-adapted sample was put in a 1-mm light-path cuvette, directly measured at room temperature or cooled down to 77 K in liquid nitrogen, and placed in a liquid-helium cryostat (Oxford Instruments, Inc., Abingdon, Oxfordshire, UK) for the measurements at low temperature.

## Data processing

### Analysis of decay profiles at each wavelength region by multi-exponential decay functions

We can obtain a series of decay kinetics of fluorescence at different-wavelength regions if we cut the 2D fluorescence profiles vertically at an interval of few tens of pixels and sum up the photon counts along the wavelength axis, as shown in Fig. 3. The calculated kinetics, then, can be further analyzed by the multi-exponential fitting program by assuming different exponential decay components. See Van Stokkum et al. (2008) and Gilmore (2004) for details of this type of analysis.

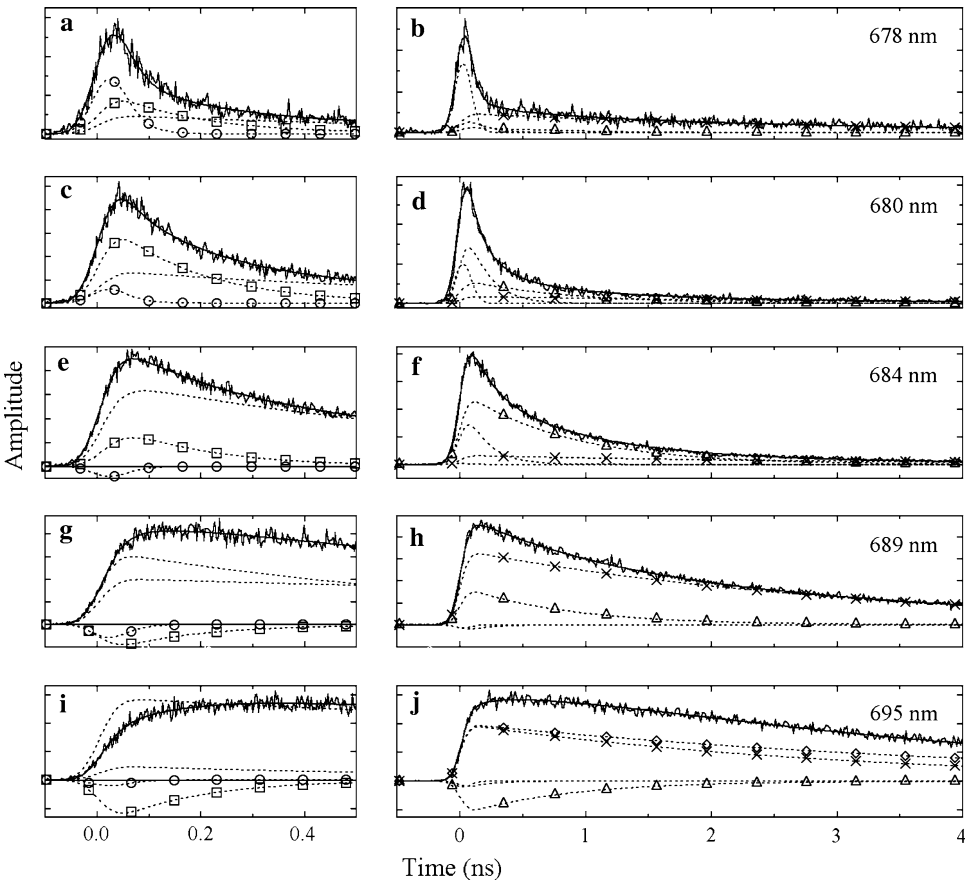


**Fig. 3** Calculation of the fluorescence decay time courses in PS II particles at selected wavelengths. **a** and **b** 678 nm, **c** and **d** 680 nm, **e** and **f** 684 nm, **g** and **h** 689 nm, and **i** and **j** 695 nm. The left panels represent the fluorescence decays obtained in the 1-ns measurement, and the right panels, those obtained in the 5-ns measurement shown in Fig. 2. The dotted lines with markers represent the estimated contribution of the decay or rise component. The amplitudes of these components are summarized as Decay Associated Spectra (DAS) in Fig. 4

### Calculation of decay associated spectrum, DAS

By analyzing the amplitudes of kinetic phases in the decay kinetics at different-wavelength regions, we can assume the spectral profiles of the same kinetic phases with common decay time constants as shown by the Decay Associated Spectrum (DAS) in Fig. 4. The DAS curve with the positive band suggests energy dissipation or the energy transfer (efflux) to the other component(s) with the calculated time constant, while the negative band suggests the energy influx from some other component. The DAS with the positive and negative bands (with the same time constant), thus, suggests that there is energy transfer from the complex giving the former band to that giving the latter band, as shown in Fig. 4.

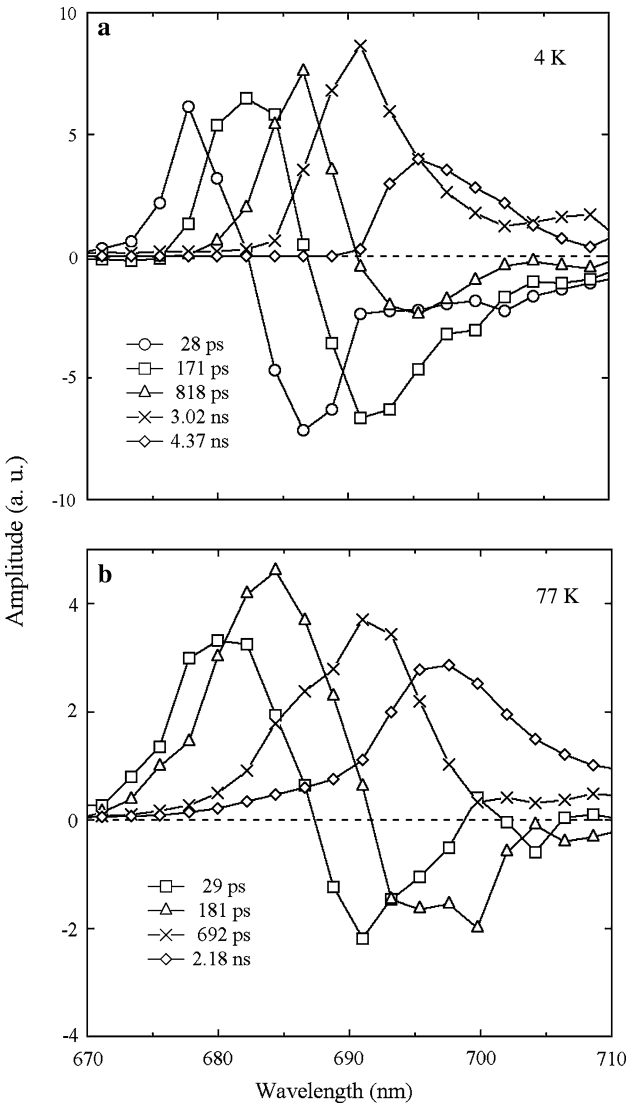


**Fig. 4** Decay Associated Spectra (DAS) calculated from the images at 4 K (**a**) or at 77 K (**b**)

### Analysis of time-resolved fluorescence spectra by a multi-Gaussian function

We can obtain a series of time-resolved fluorescence spectra, as shown in Fig. 5, if we cut the 2D fluorescence profiles horizontally into sections at an interval of few tens of pixels and sum up the photon counts along the time axis. These spectra, then, can be further analyzed by the multi-Gaussian fitting program to 'decompose' the different spectral bands (Gilmore 2004).

All the analysis was performed with respect to the wavenumber. The parameters (peak wavelength, peak height, and bandwidth) of each Gaussian component band can be fixed by a decomposition program and adjusted to give parameters common for the spectra at all delay times.

### Calculation of the decay process of each fluorescence component band

The rise and decay profiles of each component band are calculated by assuming multi-exponential decay functions. Through the search of the rise and decay of common spectral components in the decomposed time-resolved spectra, we can assume the decay profile of the same spectral components in the global analysis of the whole 2D profiles, as shown in Fig. 6. The time course gives us a more precise interpretation of the kinetic behavior and spectral features of each component band and adds more information to the DAS curve.

## An example of the fluorescence measurement and analysis: fluorescence decay process in PS II at 4–77 K

### Fluorescence decay measured by a streak camera in PS II

We describe below a measurement with isolated PS II particles as a typical case of fluorescence measurement by the streak camera photon-counting system. Figure 2 represents the typical 2D fluorescence images obtained for the PS II particles at 4 K (panel b) and 77 K (panel c) measured in the 5-ns time range. Each image was accumulated after an 1-h of measurement with the streak camera system. An image of scattering of excitation laser that has narrow spectral and time widths is also shown (panel a). The images represent the different features. This is convenient for real-time comparisons, such as the measurement of intact leaves just picked from the garden or the comparison between mutants. We can compare the image even before the detailed analysis is made, by simply looking at the accumulating pictures.

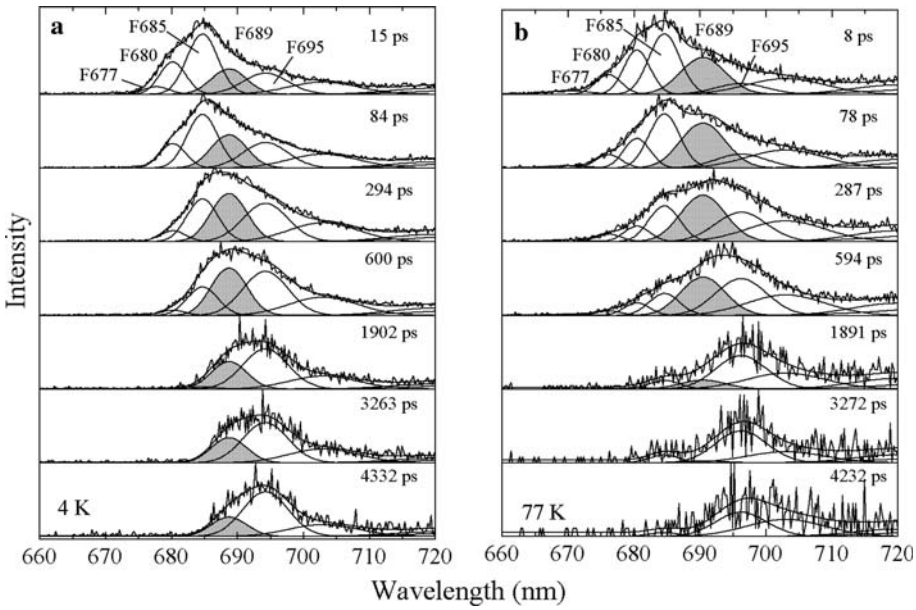


**Fig. 5** Calculation of time-resolved fluorescence spectra at 4 K (**a**) and 77 K (**b**) in PS II particles. The spectra were calculated from the experiments as those in Fig. 2. The fitted curves and component bands are shown as thin lines. F689 is highlighted with a thin black area in each spectrum. The delay time after the laser excitation is also shown

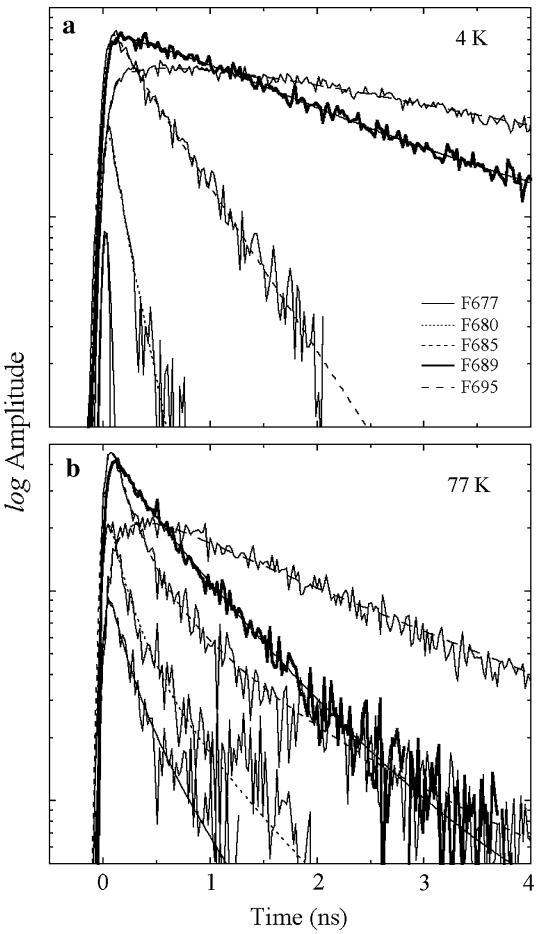


**Fig. 6** Time course of F677 (thin lines), F680 (*dotted lines*), F685 (*dashed lines*), F689 (*thick lines*), and F695 (*long-dashed lines*) obtained from Fig. 5 at 4 K (**a**) and 77 K (**b**). The smooth lines correspond to multi-exponential fitting curves

Figure 2 clearly shows the longer tails in the vertical direction of time axis at 4 K that indicates the increases of the lifetimes. These decay profiles of the fluorescence were measured with the excitation light from the 50-ps FWHM (Full Width at Half Maximum) diode laser operated at 1 MHz. The system enabled us to calculate the time course at any wavelength (see Fig. 3) and the time-resolved spectra at any delay time (see Fig. 5). At 4 K, the decay rate of the fluorescence became slower, and the contributions of the shorter-wavelength fluorescence became larger than those at 77 K, as expected from the blue shift and the enhancement of the steady-state fluorescence spectrum.

## Global analysis of the fluorescence decay process in PS II by the multi-exponential decay fitting

### Analysis of the decay profiles at 4 K

The 2D fluorescence profiles in Fig. 2 were divided into 64 wavelength regions at an interval of 2.2 nm (10 pixels). The photon counts in each division were summed up along the wavelength axis to obtain the fluorescence decay curves at each wavelength region. Figure 3 shows the typical fluorescence decay time courses at 4 K at each wavelength region between 678 and 695 nm. Generally, the blue side of the fluorescence decayed faster (e.g., at 678 and 680 nm in Fig. 3a, b, c and d), whereas the red side (e.g., at 689 and 695 nm in Fig. 3g, h, i, and j) showed distinct rising phases followed by very slow decay phases. These observations clearly indicate the characteristics of the fast downhill energy transfer from the shorter-wavelength Chls (at higher

energy levels) to the longer-wavelength Chls (at lower energy levels) in PS II. Even in the red side, the decay time courses are very different at 689 and 695 nm. The rise and decay at 695 nm are extremely slow. This complicated kinetics suggests the contributions of multiple spectral components that overlap with each other.

In the multi-exponential fitting analysis of the decay kinetics below, we analyzed two time courses at each wavelength range, which were calculated from the 1-ns and 5-ns measurements, respectively, to estimate the decay profiles over a 5-ns long period with sufficient accuracy. Five exponential decay and rise components fitted all the traces at 670–710 nm satisfactorily. The components common for all the decay time courses at different wavelengths had time constants of 28 ps, 171 ps, 818 ps, 3.02 ns, and 4.37 ns.

## Decay associated spectra at 4 K

Figure 4a shows the DAS obtained in the global multi-exponential analysis at 4 K. The three faster DAS components with time constants of 28, 171, and 818 ps show both positive and negative peaks that are indicative of the decay of one fluorescence band in parallel with the rise of another, showing the characteristics of EET. On the other hand, the two slower DAS show only positive peaks, suggesting that their decays occur only in the trapping/relaxation processes. Positive peaks were located at around 678, 682, 686, 691, and 695 nm, while negative peaks were located at around 686, 691, and 695 nm. The contributions of these DAS components to the time courses of the fluorescence at different wavelengths are shown by dotted lines in Fig. 3.

The fastest 28 ps DAS in Fig. 4a had positive and negative peaks at 678 and 686 nm, respectively, suggesting the presence of EET from the Chl form that emits at around 678 nm to another one that emits at around 686 nm. The latter seems to correspond to the F685 band. The second DAS with a 171-ps time constant had positive and negative peaks at 682 and 691 nm, respectively. The positive peak at 682 nm seems to represent F680, which is probably emitted from LHC II. The time constant, thus, represents the EET from F680 to the band that emits fluorescence at around 691 nm (tentatively designated F690 here and discussed more in depth in the following section), probably in the core antennae at 4 K. The rise and decay of the 28- and 171-ps DAS components are shown as time courses indicated by *circles* and *squares* in Fig. 3a, and c, respectively. The two DAS spectra also imply the presence of the Chl emitting at a slightly shorter-wavelength than F680; we call it F678.

The third DAS component showed a time constant of 818 ps and suggested an extremely slow EET from the component emitting 686 nm band (F685) to that emitting the 695-nm band (F695). The slow EET (plotted with *triangles* in Fig. 4a) was confirmed from the slow rise of the fluorescence at 695 nm with a peak at around 500 ps (Fig. 3f, j). The 686-nm positive peak is almost identical to that of the negative peak in the 28-ps DAS and suggested it to represent F685. These results indicate the existence of EET from component emitting F678 to that emitting F685 with a time constant of 28 ps and then from F685 to F695 with a time constant of 818 ps.

The two slow DAS components with time constants of 3.0 and 4.4 ns showed only positive peaks at 690 and 695 nm, respectively. They seemed to represent the decay through the fluorescence emission and the energy trapping by the RC Chls.

The fluorescence at 695 nm has long been known as F695, whereas fluorescence with a peak at around 690 nm has never been identified. The 690-nm positive peak in the 3.0-ns DAS corresponded well to the negative peak in the 171-ps DAS. The coincidence suggests the function of the Chl emitting at around 690 nm (F690) as a sink of excitation energy that is disconnected from F695 below 77 K.

The 4.4-ns lifetime of F695 is very slow and is close to the intrinsic lifetime of Chl *a* of $\approx$6 ns (Vlakova 2000), suggesting its function as an energy sink that does not transfer energy to the other Chls at 4 K. The 3.0-ns lifetime of F690 is also slow and it may be an energy sink that dissipates energy mainly as fluorescence. The large positive area of F690 in DAS further suggests it to be the major sink of the excitation energy at 4 K.

## Decay associated spectra at 77 K

At 77 K, only four DAS components could be identified (Fig. 4b). The 29-ps DAS component showed a broad positive peak at around 680 nm and a negative peak at around 690 nm, suggesting a faster EET rate from F680 to F690 than that of the 171 ps EET detected at 4 K. Its positive band was slightly blue-shifted and broader than that of the 171-ps DAS at 4 K. The 29-ps DAS may also include the partial contribution of the fastest component detected at 4 K. Our results suggest that the fastest 28-ps component detected at 4 K has a time constant shorter than 5 ps (below the time resolution of the present study) at 77 K. The second component at 77 K showed a time constant of 181 ps with the EET from F685 to F695. Compared to that of the 818-ps DAS component at 4 K, the positive peak of this component was also slightly blue-shifted with a broadened bandwidth and a faster decay rate (compare *triangles* in Fig. 4a to those in Fig. 4b).

The third DAS component had a time constant of 692 ps that was shorter than the corresponding time constants of 3.0 ns at 4 K. This component showed a peak at around

690 nm with almost no negative band, suggesting that the extent of the EET from F690 to F695 was small even at 77 K. Our results indicate the presence of F690 at 77 K; it is present at all the temperatures from 4 to 77 K. Although F690 is hardly observed as a distinct peak in the steady-state fluorescence spectrum at 77 K, the contribution of F690 has been detected apparently from the broadened bandwidth of F695.

The slowest DAS component at 77 K showed a time constant of 2.2 ns with a spectrum different from the slowest ones at 4 K. The main peak at 697 nm was slightly red-shifted from the 695-nm peak detected at 4 K. A small but distinct shoulder was observed at around 685 nm, suggesting that F685 and F695 decay in parallel due to the fast equilibration of excitation energy at 77 K. This equilibration process seems to become slower at 4 K.

## Global analysis of the decay process in PS II by the Gaussian decomposition of the time-resolved fluorescence spectra

We also performed another type of analysis on the same data sets. We first calculated each time-resolved fluorescence spectrum in a wavelength region from 670 to 710 nm, decomposed them into multiple Gaussian component bands, and estimated the time course of the individual component bands by global analysis. Although the time course thus estimated might be slightly erroneous because of the approximation procedure, which assumed a simple Gaussian shape for each spectral component (Kwa et al. 1994), the analysis was useful in determining the correct peak position, bandwidth, and approximate decay kinetics of each component.

### Decomposition of time-resolved fluorescence spectra into multiple spectral components

The 2D fluorescence profiles in Fig. 2 were divided either into 48 time regions at an interval of 23 ps (10 pixels) for the data set acquired in the 1-ns mode or into 240 regions at an interval of 22 ps (2 pixels) in the 5-ns mode. The time-resolved fluorescence spectrum was calculated by summing up the photon counts in each division along the time axis. Decomposition into the spectral component bands was performed on each time-resolved fluorescence spectrum from 670 to 710 nm. The parameters (peak wavelength, peak height, and bandwidth) of each Gaussian component band were selected by a home-built fitting program and were adjusted to give parameters common for all the time-resolved spectra. Then, the rise and decay profiles of each component band were calculated. All the analyses were performed with respect to wavenumbers.

We assumed six Gaussian components to fit all the time-resolved spectra at 4 and 77 K, as shown in Fig. 5. The highest-energy band, which also gave the fastest decay, showed a peak at 677 nm in every case. We designated this band as F677; it had been designated as F678 in the previous section. Three additional bands at 680, 685, and 695 nm were identified in all decomposition analyses and were assigned to F680, F685, and F695, respectively. In addition, a band peaking at 689 nm at 4 K and at 690 nm at 77 K was also obtained and was designated as F689 (or F690). We assumed one extra minor compensation band at around 703 nm to optimize the fitting in all cases. This band could be an extra fluorescence component emitting from some Chl-binding proteins, such as LHC II aggregates (they emit fluorescence peaking at around 700 nm; see Horton et al. 1991).

Figure 5 summarizes the spectral components analyzed in each time-resolved spectrum, in which F689 (F690) is highlighted by a shadowed curve. Within a hundred ps after the laser excitation, F677, F680, and F685 gave contributions higher than F689 and F695. The apparent peak wavelength of each time-resolved spectrum shifted to the red with time, indicating slow evolution of F689 and F695 bands. At 4 K, bands other than F689 and F695 almost disappeared after 2 ns. F689 decayed faster than F695. F695, thus, is the lowest energy sink in PS II and is the major contributor to the steady-state fluorescence spectrum at 4 K because of the slowest decay.

At 77 K, the kinetics in the longer time domain was significantly different. Apparent peaks of time-resolved spectra shifted to the red with time. F689 decayed more rapidly and almost disappeared after 3 ns. On the other hand, a small contribution of F685 still remained even after 4 ns. Therefore, only F685 and F695, but not F689, can be clearly noticed in the steady-state fluorescence spectrum at 77 K. However, the contribution of F689 to the steady-state fluorescence produces the broad F695 band. This is consistent with the reports of wide F695 bandwidths in earlier studies (Gilmore et al. 2000, 2003a).

### Decay kinetics of each spectral component band

The time-dependent change of the amplitude of each band was simulated as shown in Fig. 6. At 4 K, the lower (redder) the energy level of fluorescence bands, the lower the decay rate. Each band, except F689 and F695, showed an almost single-exponential decay indicating the downhill EET toward the lower energy states at 4 K. F689 and F695 showed distinctive slow rises indicating energy transfer from the other Chl bands.

At 77 K, the decay rates of all the components were accelerated. F685 and F695 appeared to decay almost in parallel after 2 ns, suggesting the fast equilibration of the

excitation energy between them. On the other hand, the decay of F689 (thick line) was faster and independent from those of F685 and F695. This strongly suggests that the EET between F689 and F685 or that between F689 and F695 is slow below 77 K, in agreement with a conclusion reached in global multi-exponential analysis.

## Tentative scheme of the excitation energy transfer in PS II at 4–77 K

Through the two independent methods of analyses of the 2D fluorescence profiles measured at 4–77 K by the streak camera system, we have identified a new fluorescence band, F689, besides the well-known F680, F685, and F695 bands in spinach PS II particles. The blue shift of the steady-state fluorescence spectrum that was detected upon cooling below 77 K can be interpreted as the increase of the fluorescence emission from the shorter-wavelength Chl bands, especially F689. The slowdown of the EET process also increased the chance to emit fluorescence from the shorter-wavelength Chls. F685 and F695 seem to be thermally equilibrated rapidly at 77 K but not at 4 K. We propose a tentative scheme of EET at 4 K (Fig. 7) based on the results discussed in this article. The scheme with the significantly longer EET time constants and the presence of F689 explain the higher probability of fluorescence emission from the short-wavelength fluorescence bands. This mechanism seems to interpret the blue shift of the steady-state fluorescence on cooling below 77 K. The analysis of the fluorescence decay at 4 K in PS II revealed (1) a new band, F689, (2) the mechanism of the blue shift of the steady-state fluorescence spectrum due to the significantly slower EET rates, (3) the pathways of down-hill EET in the complex, and (4) the fact that the EET pathways that stop at 4 K seem to contain uphill EET steps.

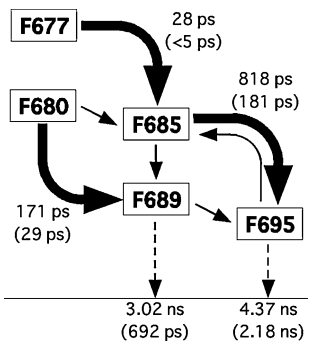


**Fig. 7** Estimated scheme of excitation energy transfer among the fluorescence component bands in PS II based on the 2D fluorescence measurements at 4–77 K. The bold arrows represent the major energy transfer pathways. The estimated time constants of the excitation energy transfer/relaxation at 4 K; 77 K time constants are shown in parentheses

The analysis with the streak camera gives high-quality information that provides the basis for the multiple analyses presented here.

## 2D fluorescence images in various systems

The measurement of the 2D fluorescence image of the decay/spectrum by the single-photon-counting streak camera system is rather simple if the proper instrumentation is available. We can usually obtain a fine image within 1 h with a small amount of sample if they fluoresce like chloroplasts. After obtaining images, we can proceed to an extensive analysis, if necessary. These features make the measurement system suitable for comparison of fluorescence between different organisms, the screening of mutant strains, or the analysis of effects of reagents, temperature, stress, and damage. We can measure a clear emission spectrum of the fast-decaying fluorescence component together with the slow-decaying components that mainly contribute to the steady-state fluorescence. The measurement is sometimes even easier than the measurement with an ordinary fluorometer.

We present 2D fluorescence images of different samples at different temperatures obtained by the streak camera system in Figs. 8 and 9. These images clearly show the unique features of the samples.

### Fluorescence from intact leaf of *A. thaliana* at 4–77 K

*Arabidopsis thaliana* is widely used as one of the most useful model plants. We measured the fluorescence from a small spot on the upper surface of a leaf in *A. thaliana* at 4–77 K. A piece of leaf was fixed with cotton in a 1-cm light-path cuvette. The cuvette was soaked into liquid nitrogen to be cooled rapidly to 77 K and then it was placed in a liquid-helium cryostat. The excitation source was a 405-nm laser diode, and the fluorescence at 635–775 nm was detected.

Figures 8a and 8b show the fluorescence images measured in the 5 ns time range at 4 and 77 K, respectively. The images had two intense regions that originated from PS II (670–700 nm) and PS I (710–775 nm), respectively. The fluorescence of PS I has a single broad band from a so-called red Chl peaking at around 735 nm at both 4 and 77 K. The red Chl species seem to be bound in one of the peripheral antenna proteins, LHC I. Upon warming from 4 K to 77 K, the fluorescence decay of PS I was only slightly accelerated. The PS II fluorescence, on the other hand, was drastically changed upon warming to 77 K showing the red shift of the peak. The results are similar to those seen with the isolated spinach PS II particles that are shown in Figs. 2b and 2c and suggest the common EET mechanisms in PS II in higher plants.

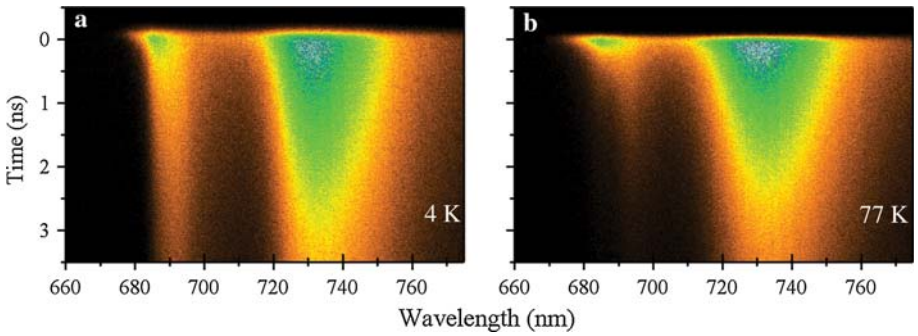


**Fig. 8** Temperature dependence of the 2D fluorescence images of an *A. thaliana* leaf. The measuring temperature was at 4 K (**a**) and at 77 K (**b**). The excitation source was a 405-nm laser diode operated at 1 MHz. See text for details

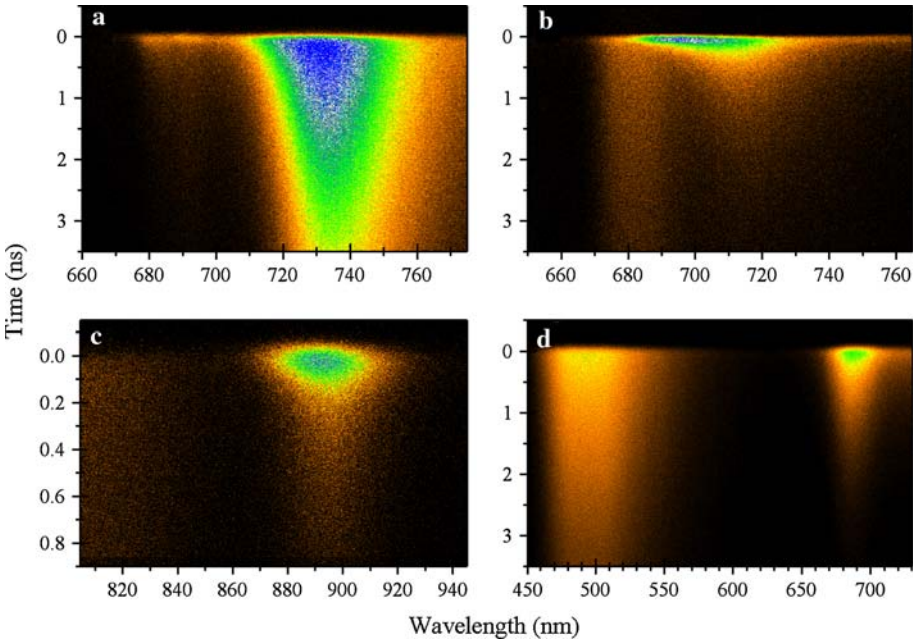


**Fig. 9** **a**. 2D fluorescence image at 4 K of PS I particles isolated from spinach. The excitation light source was a 405-nm laser diode operated at 1 MHz. **b**. 2D fluorescence image at 77 K of the FCP-PS I supercomplex isolated from a marine centric diatom, *C. gracilis*. The fluorescence measurement was performed with a 460-nm, 120-femtosecond laser flash that excited Chl *c* mainly. **c**. 2D fluorescence image at 77 K of isolated membranes from a purple photosynthetic bacterium, *A. rubrum*, which has Zn-bacteriochlorophyll *a* in contrast to all the other photosynthetic bacteria that use Mg-bacteriochlorophyll *a*. The excitation light source was a 405-nm laser diode operated at 1 MHz. **d**. 2D fluorescence image at room temperature in a living coral with an intrinsic green fluorescent protein (GFP) and an endosymbiont, *Zooxanthella*. The long-decay fluorescence at 400–500 nm comes from GFP and the fast-decay fluorescence at around 680 nm comes from Chls in *Zooxanthella.* The excitation light source was a 405-nm laser diode operated at 1 MHz. Details of the experimental conditions for the measurements are given in the text

## Fluorescence of PS I complex isolated from spinach at 4 K

Figure 9a shows the 4-K fluorescence of isolated spinach PS I particles. Similar to the fluorescence images of *A. thaliana* (Fig. 8a), a slow decay of strong fluorescence of red Chl was observed at 735 nm at 4 K. At 670–700 nm, a rapid decay of fluorescence was observed, indicating the fast EET from the bulk shorter-wavelength Chls to the red Chl. Two small bands can be seen at around 680 and 690 nm. These bands indicate the heterogeneity of bulk Chls, which are difficult to detect at 77 K or higher temperatures.

## Fluorescence of Fucoxanthin Chlorophyll Proteins -PS I complex isolated from a diatom, *C. gracilis* at 77 K

Diatoms perform about 40% of the photosynthetic carbon fixation in the oceans, which corresponds to 20% of the global primary production. However, little is known about the photosynthetic system of the diatom. We measured the fluorescence of highly photoactive thylakoid membranes

and the PS I complex isolated from a marine centric diatom, *C. gracilis* (Ikeda et al. 2008). The purified PS I complex contained tightly bound fucoxanthin chlorophyll proteins (FCPs) that bind Chl *c* and Chl *a* and transfer excitation energy to PS I. A 2D fluorescence measurement was performed at 77 K with the 460-nm, 120-fs laser flash to excite Chl *c* directly. Figure 9b shows the 2D fluorescence image of the FCP-PS I supercomplex excited at 460 nm at 77 K. A very fast decay, compared to that of the spinach PS I, was observed. This suggests fast EET from FCP to PS I and a fast excitation energy trapping inside PS I of a diatom even at 77 K, as discussed elsewhere (Ikeda et al. 2008).

Although most photosynthetic organisms reveal a 720–730 nm PS I fluorescence band from the red Chl *a*, some species lack the red Chl. The PS I fluorescence bands then overlap with PS II fluorescence bands. On the other hand, oligomerization of PS I trimer, such as induced by a depletion of a lipid phosphatidylglycerol affect the fluorescence spectrum (Domonkos et al. 2004). Under these conditions, the lifetime measurement by the streak camera system is very informative, as reviewed by Itoh and Sugiura (2004).

### Fluorescence at 77 K of membranes isolated from cells of a purple photosynthetic bacterium, *A. rubrum*, which uses Zn-bacteriochlorophyll *a*

A purple acidophilic photosynthetic bacterium, *A. rubrum*, is a unique photosynthetic organism that has bacteriochlorophyll *a* containing Zn as a central metal instead of Mg (Wakao et al. 1996) and the electron acceptor bacteriopheophytin *a*. The bacterium has a type-II RC surrounded by an antenna protein complex called light-harvesting complex 1 (LH1), as do many other purple bacteria. We isolated the membranes from the cells and studied the fluorescence mainly emitted from LH I in the presence of sodium ascorbate to reduce the electron donor Zn-bacteriochlorophyll *a* special pair at 77 K. The excitation light source was a 405-nm laser diode. Figure 9c shows the fluorescence emission of Zn-bacteriochlorophyll *a* in LH1 at around 890 nm in the 1-ns measurement (T. Tomi et al. unpublished data 2009). The peak wavelength of the LH1 fluorescence is about 5 nm shorter than the LH1 of the other purple bacteria that have Mg-bacteriochlorophyll *a*. The main decay time constant was 47 ps, suggesting that the EET from LH1to RC takes place rapidly. As reported by Tomi et al. (2007), the EET and the electron transfer process in *A. rubrum* that has Zn-bacteriochlorophyll *a* occurs in a manner that is essentially similar to that in other purple photosynthetic bacteria that use Mg-bacteriochlorophyll *a*. 2D images of fluorescence from bacteriochlorophylls *a* and *c* were also reported in a mutant strain of a green sulfur bacterium, *Chlorobium tepidum* (Tsukatani et al. 2004).

### Fluorescence at room temperature of a coral with intrinsic green fluorescent protein (GFP) and an endosymbiont, *Zooxanthella*

As an extreme case, we also studied in situ fluorescence of corals that have an algal endosymbiont, *Zooxanthella*, to investigate the role of GFP in the photosynthesis of *Zooxanthella* (Gilmore et al. 2003b). We used a grating of 50 grooves $mm^{-1}$ to cover a wide range of emission wavelengths to detect the fluorescence of GFP and Chl *a* simultaneously. The excitation light source was a 405-nm laser diode. Figure 9d shows the fluorescence of GFP (emission at around 500 nm) and Chl *a* in PS II of *Zooxanthella* (at around 680 nm) at room temperature. As seen in the image, the fluorescence of GFP showed a slower decay than the Chl *a* fluorescence. Spectral and kinetic analyses of the fluorescence revealed no detectable EET from GFP to PS II (Gilmore et al. 2003b). We concluded that GFP does not function as the extra antenna to PS II and that GFP could only indirectly work to absorb, screen, and scatter UV–blue light to protect PS II.

## Conclusions

Fluorescence lifetime measurements with a streak camera system operated in the photon-counting mode provide a compact, convenient, and a high-quality method for studying fluorescence. We used this system to analyze a wide variety of photosynthetic systems, including intact leaves, intact cells of cyanobacteria, cells in a single colony, and pigment protein complexes purified from various organisms including green plants, algae (green, brown, and red), cyanobacteria, anoxygenic photosynthetic bacteria (purple bacteria, and green sulfur bacteria) in a wavelength range from 400 nm to 900 nm. The system has been easily adapted to non-photosynthetic systems, such as flavin (Fukushima et al. 2005), green fluorescent proteins, or porphyrins. Most of these materials could be measured with simple excitation using a laser diode or a femtosecond laser. The measurement at the cryogenic temperature, especially at 4 K, makes the energy transfer time longer and offers better analysis of the ultra-fast EET process, as shown in this review.

The 2D images obtained by the system can be directly compared to assess the differences even without the requirement of deep knowledge of the fluorescence mechanism itself. Detailed analyses can also be performed, if required, as shown in this review. It might be useful, in the future, to make a free-access data bank that is full of 2D

fluorescence images of different photosynthetic organisms measured under various conditions.

**Acknowledgments** This study was supported by a COE program for "The origin of the universe and matter" and by a grant-in-aid (No. 17370055) from the Japanese Ministry of Education, Science, Sports, and Culture to S·I. We are grateful to Mrs. Y. Nakamura and Drs. T. Tomi, Y. Shibata, H. Mino, A.M. Gilmore, Govindjee, A.W.D. Larkum, Z. Gombos, and Y. Ikeda who gave us a chance to measure variety of samples. We thank Govindjee for editing this manuscript.

## References

Amunts A, Drory O, Nelson N (2007) The structure of a plant photosystem I supercomplex at 3.4 Å resolution. Nature 447:58–63

Andrizhiyevskaya EG, Frolov D, van Grondelle R, Dekker JP (2004) On the role of the CP47 core antenna in the energy transfer and trapping dynamics of photosystem II. Phys Chem Chem Phys 6:4810–4819

Andrizhiyevskaya EG, Chojnicka A, Bautista JA, Diner BA, van Grondelle R, Dekker P (2005) Origin of the F685 and F695 fluorescence in photosystem II. Photosynth Res 84:173–180

Berthold DA, Babcock GT, Yocum CF (1981) A highly resolved, oxygen-evolving photosystem II preparation from spinach thylakoid membranes: EPR and electron-transport properties. FEBS Lett 134:231–234

Boekema EJ, van Roon H, Calkoen F, Bassi R, Dekker JP (1999) Multiple types of association of photosystem II and its light-harvesting antenna in partially solubilized photosystem II membranes. Biochemistry 38:2233–2239

Brody SS, Brody M (1963) Aggregated chlorophyll in vivo. Natl Acad Sci-Natl Res Council Publ 1145:455–478

Broess K, Trinkunas G, van der Weij-de Wit CD, Dekker JP, van Hoek A, van Amerongen H (2006) Excitation energy transfer and charge separation in photosystem II membranes revisited. Biophys J 91:3776–3786

Cho F, Govindjee (1970a) Low temperature (4–77 K) spectroscopy of Chlorella: temperature dependence of energy transfer efficiency. Biochim Biophys Acta 216:139–150

Cho F, Govindjee (1970b) Low temperature (4–77 K) spectroscopy of Anacystis: temperature dependence of energy transfer efficiency. Biochim Biophys Acta 216:151–161

Cho F, Spencer J, Govindjee (1966) Emission spectra of *Chlorella* at very low temperatures (−269 to −196°C). Biochim Biophys Acta 126:174–176

Croce R, Dorra D, Holzwarth AR, Jennings RC (2000) Fluorescence decay and spectral evolution in intact photosystem I of higher plants. Biochemistry 39:6341–6348

De Weerd FL, Palacios MA, Andrizhiyevskaya EG, Dekker JP, Van Grondelle R (2002a) Identifying the lowest electronic states of the chlorophylls in the CP47 core antenna protein of photosystem II. Biochemistry 41:15224–15233

De Weerd FL, van Stokkum IHM, van Amerongen H, Dekker JP, Van Grondelle R (2002b) Pathways for energy transfer in the core light-harvesting complexes CP43 and CP47 of photosystem II. Biophys J 82:1586–1597

Dekker JP, van Grondelle R (2001) Primary charge separation in photosystem II. Photosynth Res 63:195–208

Dekker JP, Jassoldt A, Pettersson A, van Roon H, Groot ML, van Grondelle R (1995) On the nature of the F695 and F685 emission of photosystem II. In: Mathis P (ed) Photosynthesis: from light to biosphere, vol 1. Kluwer, Dordrecht, pp 53–56

Domonkos I, Malec P, Sallai A, Kovács L, Itoh K, Shen G, Ughy B, Bogos B, Sakurai I, Kis M, Strzalka K, Wada H, Itoh S, Farkas T, Gombos Z (2004) Phosphatidylglycerol is essential for oligomerization of photosystem I reaction center. Plant Physiol 134:1471–1478

Fleming GR, Morris JM, Robinson GW (1977) Picosecond fluorescence spectroscopy with a streak camera. Austr J Chem 30:2338–2352

Fukushima Y, Okajima K, Shibata Y, Ikeuchi M, Itoh S (2005) Primary intermediate in the photocycle of a blue-light sensory BLUF FAD-protein, Tll0078, of *Thermosynechococcus elongatus* BP-1. Biochemistry 44:5149–5158

Gasanov R, Abilov ZK, Gazanchyan RM, Kurbonova UM, Khanna R, Govindjee (1979) Excitation-energy transfer in photosystem-I and photosystem-II from grana and in photosystem-I from stroma lamellae, and identification of emission bands with pigment-protein complexes at 77 K. Z Pflanzenphysiol 95:149–169

Gilmore AM (2004) Excess light stress: Probing excitation dissipation mechanisms through global analysis of time- and wavelength-resolved chlorophyll *a* fluorescence. In: Papageorgiou GC, Govindjee (eds) Chlorophyll *a* fluorescence: a signature of photosynthesis. Dordrecht, Springer

Gilmore AM, Itoh S, Govindjee (2000) Global spectral-kinetic analysis of room temperature chlorophyll a fluorescence from light-harvesting antenna mutants of barley. Philos Trans R Soc Lond B 355:1371–1384

Gilmore AM, Matsubara S, Ball MC, Barker DH, Itoh S (2003a) Excitation energy flow at 77 K in the photosynthetic apparatus of overwintering evergreens. Plant Cell Environ 26:1021–1034

Gilmore AM, Larkum AWD, Salih A, Itoh S, Shibata Y, Bena C, Yamasaki H, Papina M, van Woesik R (2003b) Simultaneous time resolution of the emission spectra of fluorescent proteins and *Zooxanthella* Chlorophyll in reef-building corals. Photochem Photobiol 77:515–523

Gobets B, Van Grondelle R (2001) Energy transfer and trapping in photosystem I. Biochim Biophys Acta 1507:80–99

Gobets B, Stokkum IHM, Rögner M, Kruip J, Schlodder E, Karapetyan N, Dekker JP, van Grondelle R (2001) Time-resolved fluorescence emission measurements of photosystem I particles of various cyanobacteria: a unified compartmental model. Biophys J 81:407–424

Govindjee, Yang L (1966) Structure of the red fluorescence band in chloroplasts. J Gen Physiol 49:763–780

Govindjee, Amesz J, Fork DC (eds) (1986) Light emission by plants and bacteria. Academic Press, Orlando

Groot ML, Peterman EJG, Van Kan PJM, Van Stokkum IHM, Dekker JP, Van Grondelle R (1994) Temperature-dependent triplet and fluorescence quantum yields of the photosystem II reaction center described in a thermodynamic model. Biophys J 67:318–330

Groot ML, Peterman EJG, van Stokkum IHM, Dekker JP, Van Grondelle R (1995) Triplet and fluorescing states of the CP47 antenna complex of photosystem II studied as a function of temperature. Biophys J 68:281–290

Groot ML, Frese RN, de Weerd FL, Bromek K, Pettersson Å, Peterman EJG, van Stokkum IHM, van Grondelle R, Dekker JP (1999) Spectroscopic properties of the CP43 core antenna protein of photosystem II. Biophys J 77:3328–3340

Guskov A, Kern J, Gabdulkhakov A, Broser M, Zouni A, Saenger W (2009) Cyanobacterial photosystem II at 2.9-Å resolution and the role of quinones, lipids, channels and chloride. Nature Struct Mol Biol 16:334–342

Horton P, Ruban AV, Rees D, Pascal AA, Noctor G, Young AJ (1991) Control of the light-harvesting function of chloroplast membranes by aggregation of the LHCII chlorophyll-protein complex. FEBS Lett 292:1–4

Ihalainen JA, Van Stokkum IHM, Gibasiewicz K, Germano M, Van Grondelle R, Dekker JP (2005) Kinetics of excitation trapping in intact photosystem I of *Chlamydomonas reinhardtii* and *Arabidopsis thaliana*. Biochim Biophys Acta 1706:267–275

Ikeda Y, Komura M, Watanabe M, Minami C, Koike H, Itoh S, Kashino Y, Satoh K (2008) Photosystem I complexes associated with fucoxanthin-chlorophyll-binding proteins from a marine centric diatom, *Chaetoceros gracilis*. Biochim Biophys Acta 1777:351–361

Ito T, Hiramatsu M, Hosoda M, Tsuchiya Y (1991) Picosecond time-resolved absorption spectrometer using a streak camera. Rev Sci Instrum 62:1415–1419

Itoh S, Sugiura K (2004) Photosystem I fluorescence. In: Papageorgiou GC, Govindjee (eds) Chlorophyll *a* fluorescence: a signature of photosynthesis. Dordrecht, Springer

Jordan P, Fromme P, Witt HT, Klukas O, Saenger W, Krauβ N (2001) Three-dimensional structure of cyanobacterial photosystem I at 2.5 Å resolution. Nature 411:909–917

Komura M, Shibata Y, Itoh S (2006) A new fluorescence band F689 in photosystem II revealed by picosecond analysis at 4–77 K: function of two terminal energy sinks F689 and F695 in PS II. Biochim Biophys Acta 1757:1657–1668

Krausz E, Hughes JL, Smith PJ, Pace RJ, Årsköld SP (2005) Assignment of the low-temperature fluorescence in oxygen-evolving photosystem II. Photosynth Res 84:193–199

Krey A, Govindjee (1964) Fluorescence change in *Porphyridium* exposed to green light of different intensity: a new emission band at 693 nm and its significance to photosynthesis. Proc Natl Acad Sci USA 52:1568–1572

Kwa SLS, Volker S, Tilly NT, van Grondelle R, Dekker JP (1994) Polarized site-selection spectroscopy of chlorophyll *a* in detergent. Photochem Photobiol 59:219–228

Loll B, Kern J, Saenger W, Zouni A, Biesiadka J (2005) Towards complete cofactor arrangement in the 3.0 Å resolution structure of photosystem II. Nature 438:1040–1044

Masters V, Smith PJ, Krausz E, Pace R (2001) Stark shifts and exciton coupling in PSII 'Supercores'. J Lumin 94–95:267–270

Melkozernov AN (2001) Excitation energy transfer in photosystem I from oxygenic organisms. Photosyn Res 70:129–153

Miloslavina Y, Szczepaniak M, Müller MG, Sander J, Nowaczyk M, Rögner M, Holzwarth AR (2006) Charge separation kinetics in intact photosystem II core particles is trap-limited. A picosecond fluorescence study. Biochemistry 45:2436–2442

Mimuro M, Tamai N, Yamazaki T, Yamazaki I (1987) Excitation energy transfer in spinach chloroplasts. FEBS Lett 213:119–122

Mino H, Itoh S (2005) EPR properties of a g = 2 broad signal trapped in S1 state in the $Ca^{2+}$-depleted photosystem II. Biochim Biophys Acta 1708:42–49

Murata N, Nishimura M, Takamiya A (1966) Fluorescence of chlorophyll in photosynthetic system. III. Emission and action spectra of fluorescence-three emission bands of chlorophyll a and the energy transfer between two pigment systems. Biochim Biophys Acta 126:234–243

Ono T, Inoue Y (1986) Effects of removal and reconstitution of the extrinsic 33, 24 and 16 kDa proteins on flash oxygen yield in photosystem II. Biochim Biophys Acta 850:380–389

Papageorgiou GC, Govindjee (eds) (2004) Chlorophyll *a* fluorescence: a signature of photosynthesis. Springer, Dordrecht

Slavov C, Ballottari M, Morosinotto T, Bassi R, Holzwarth R (2008) Trap-limited charge separation kinetics in higher plant photosystem I complexes. Biophys J 94:3601–3612

Tomi T, Shibata Y, Ikeda Y, Taniguchi S, Haik C, Mataga N, Shimada K, Itoh S (2007) Energy and electron transfer in the photosynthetic reaction center complex of *Acidiphilium rubrum* containing Zn-bacteriochlorophyll a studied by femtosecond up-conversion spectroscopy. Biochim Biophys Acta 1767:22–30

Tsukatani Y, Miyamoto R, Itoh S, Oh-Oka H (2004) Function of a PscD subunit in a homodimeric reaction center complex of the photosynthetic green sulfur bacterium *Chlorobium tepidum* studied by insertional gene inactivation. Regulation of energy transfer and ferredoxin-mediated $NADP^+$ reduction on the cytoplasmic side. J Biol Chem 279:51122–51130

Van Dorssen RJ, Plijter JJ, Dekker JP, Den Ouden A, Amesz J, Van Gorkom HJ (1987a) Spectroscopic properties of chloroplast grana membranes and of the core of photosystem II. Biochim Biophys Acta 890:134–143

Van Dorssen RJ, Breton J, Plijter JJ, Satoh K, Van Gorkom HJ, Amesz J (1987b) Spectroscopic properties of the reaction center and of the 47-kDa chlorophyll protein of photosystem II. Biochim Biophys Acta 893:267–274

Van Stokkum IHM, van Oort B, van Mourik F, Gobets B, van Amerongen H (2008) (Sub)-picosecond spectral evolution of fluorescence studied with a Synchroscan streak-camera system and target analysis. In: Aartsma TJ, Matysik J (eds) Biophysical techniques in photosynthesis (Advances in Photosynthesis and Respiration), vol 26. Springer, Dordrecht, pp 223–240

Vlakova R (2000) Chlorophyll a self-assembly in polar solvent-water mixtures. Photochem Photobiol 71:71–83

Wakao N, Yokoi N, Isoyama N, Hiraishi A, Shimada K, Kobayashi M, Kise H, Iwaki M, Itoh S, Takaichi S, Sakurai Y (1996) Discovery of natural photosynthesis using Zn-containing bacteriochlorophyll in an aerobic bacterium *Acidiphilium rubrum*. Plant Cell Physiol 37:889–893